Eur. Phys. J. D **13**, 165–180 (2001)

THE EUROPEAN PHYSICAL JOURNAL D

EDP Sciences
© Società Italiana di Fisica
Springer-Verlag 2001

Experimental and theoretical analysis of the 5pnp J = 0e, 1e, 2e autoionizing spectrum of Sr

S. Cohen[1], M. Aymar[2], A. Bolovinos[3,a], M. Kompitsas[4], E. Luc-Koenig[2], H. Mereu[2,b], and P. Tsekeris[3]

[1] Institute of Accelerating Systems and Applications, P.O. Box 17214, 10024 Athens, Greece
[2] Laboratoire Aimé Cotton, CNRS II, bâtiment 505, 91405 Orsay Cedex, France
[3] Atomic and Molecular Physics Laboratory, Physics Department, University of Ioannina, 45110 Ioannina, Greece
[4] Theoretical and Physical Chemistry Institute, National Hellenic Research Foundation, 48 Vasileos Constantinou avenue, 11635 Athens, Greece

Received 31 May 2000

Abstract. The even parity $5pnp\,J = 0$, 1 and 2 doubly excited autoionizing states of strontium were investigated both experimentally and theoretically. Sr atoms in an atomic beam were excited through the two-step Isolated Core Excitation (ICE) scheme $5s^2\ {}^1\mathrm{S}_0 - \lambda_1 \rightarrow 5sn'p\ {}^1\mathrm{P}_1\ (n' = 12{-}16) - \lambda_2 \rightarrow [5p_{3/2}np]_J$. The final ICE transition probes the $[5p_{3/2}np]_J$ resonances. However, the $[5p_{1/2}np]_J$ series below the $5p_{1/2}$ threshold were excited also due to their mixing with the $[5p_{3/2}np]_J$ perturbers. An extended energy region was covered below and above the $5p_{1/2}$ ionization limit by saturating the central ICE lobe and recording as many as possible "red" and "blue" secondary lobes. J identification was achieved by using mutually parallel and perpendicular linear polarizations of the laser beams. The ICE spectra were compared to those obtained by employing a two-step excitation scheme using the bound $4d5p\ {}^1\mathrm{P}_1$ valence state as an intermediate one. Final identification for very complex structures was achieved after comparison with theoretical energy level positions and excitation profiles produced by the R-matrix method combined with the multichannel quantum defect theory (MQDT) method. The agreement between theoretical and observed structures is quite satisfactory.

PACS. 32.80.Rm Multiphoton ionization and excitation to highly excited states (e.g., Rydberg states) – 32.30.Jc Visible and ultraviolet spectra – 32.80.Dz Autoionization

1 Introduction

Alkaline earth atoms are nowadays the systems where doubly excited autoionizing Rydberg series have been most intensively investigated, both experimentally and theoretically. The fact that they possess two ground state ms^2 valence electrons ($m = 4$, 5 and 6 for Ca, Sr and Ba respectively) lying outside closed shells makes them ideal simulators of two-electron systems. Moreover, the excitation of the two valence electrons to Rydberg series converging towards the lower lying limits above the first ionization threshold requires visible or nearly-visible radiation which is both easily produced by conventional laser systems and incapable to excite the closed shells. Theoretically, too, the application of the R-matrix method in conjunction with multichannel quantum defect theory (MQDT) led to the reproduction of energy level positions, autoionization widths and excitation profiles to nearly spectroscopic accuracy [1]. The wealth of spectroscopic data and theoretical calculations for the lowest lying autoionizing $(m{-}1)dnl$ Rydberg series in Ca [1,2], Sr [1,3–5] and Ba [1,6] is such that allows electron correlation trends among spectra of the same configuration and symmetry to be traced.

Above the $(m-1)d_j$ ionization limits, the level structure is dominated by the $mpnl$ doubly excited configurations, the practical importance of which in autoionization-pumped lasers and lasing without inversion processes has long ago been pointed out [7]. The study of odd parity states was based on either ground state photoionization [8], or multistep laser excitation schemes [9,10]. Concerning the even parity spectrum, the $mpnp$ series are of particular interest because they constitute a manifold of autoionizing states involving a limited number of J components, ranging from $J = 0$ to $J = 3$ and giving rise to a total of ten Rydberg series. Using a two-step excitation scheme from the ground state all J-components can be populated, with the exception of the one with $J = 3$, thus providing information on the manifold as a whole. Additionally, by varying the linear polarizations of the required two laser beams from mutually parallel to mutually perpendicular, J identification can, in principle,

[a] e-mail: abolovin@cc.uoi.gr
[b] *Present address:* Systèmes dynamiques, énergétiques et méchaniques, Équipe ondes et accoustique, Faculté de Corté, 20250 Corté, France.

be achieved. The $[mp_{1/2,3/2}np]_{J=0,1,2}$ series have so far been studied experimentally and theoretically in Ba [11, 12] and, more recently, in Ca [13]. In Sr only a few of the lowest members of these series were found to be located either below the $5s_{1/2}$ threshold ($5p^2\,{}^3P_{0,1,2}$) or between the $5s_{1/2}$ and $4d_{3/2}$ limits ($5p^2\,{}^1D_2$, ${}^1S_0$ and $5p6p\,{}^3P_{0,1,2}, {}^1P_1, {}^1D_2, {}^3S_1, {}^3D_{1,2,3}$) [4,5]. The main purpose of the present paper is to extend the observation of the Sr $5p_{1/2,3/2}np$, $J = 0, 1, 2$ series above the $4d_{5/2}$ limit, in order to complete the spectroscopy and analysis of the alkaline earth $[mpnp]_{J=0,1,2}$ series and permit the examination of electron correlation systematics.

Among the possible two-step excitation schemes by which final states with $J = 0, 1, 2$ and converging to the $mp_{1/2,3/2}$ ionization thresholds may be reached, we may choose either the Isolated Core Excitation (ICE) method or one involving an intermediate bound state of valence character. The ICE technique relies on the sequential excitation of the two valence electrons. The atoms are first transferred to a bound Rydberg $msn'p$ state, while the second $msn'p \rightarrow mp_jnp$ step is a transition between Rydberg states (essentially an ionic $ms \rightarrow mp_j$ core transition). The major advantage of ICE is the suppression of continuum excitation [9,10]. ICE spectra typically exhibit a characteristic excitation envelope which is composed of a strong central lobe followed by much weaker "red" and "blue" secondary lobes (satellites) separated by points of negligible absorption ("zeros"). Usually only the spectrum within the central lobe is considered since the structures within the satellites suffer from low intensity and are deformed near the zeros. The most straightforward method of recording those weaker parts of the spectrum is by shifting the central lobe (*i.e.* by changing the intermediate Rydberg state). In the case that the necessary laser wavelengths are not available, one may record the so-called "Power-spectrum" [9], *i.e.* use enough laser intensity to saturate the central lobe and observe as many satellites as possible. Still the spectrum will suffer from the ICE envelope zeros.

These last complications are not encountered in the spectra recorded through an intermediate state of valence character. In this case the complete spectrum may be obtained in a continuous frequency scan and zeros do not appear, except when caused by interference effects. More important, strong transitions are generally observed between a valence intermediate state and the first lower lying members of the final Rydberg series. The latter possess valence rather than Rydberg character and therefore the ICE technique is not very suitable for their investigation, since its second step involves a transition between Rydberg states. On the other hand, valence excitation does not impose any particular filtering of the final closed and open channels accessible to direct excitation. From the theoretical point of view, a successful reproduction of the absorption cross-section relies heavily on the proper description of the intermediate valence state wavefunction, which is often highly correlated, when both valence electrons have comparable excitation energies.

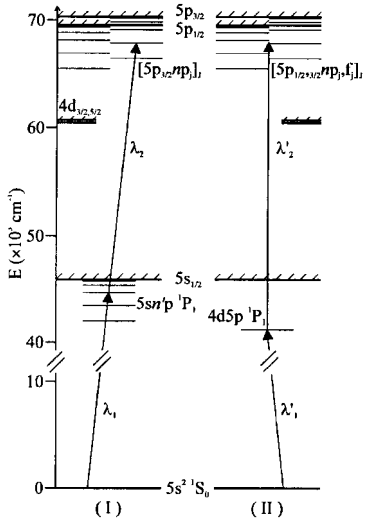

Fig. 1. Energy level diagram of Sr showing the two-step excitation paths: (I) ICE scheme through the $5sn'p\ {}^1P_1$ ($n' = 12-16$) bound Rydberg intermediate states. (II) Valence scheme through the bound $4d5p\ {}^1P_1$ intermediate state at 41 172.15 cm^{-1}.

In this work the lower lying $[5pnp]_{J=0,1,2}$ members were reached exclusively through the doubly excited $4d5p\ {}^1P_1$ bound state using the excitation scheme: $5s^2\,{}^1S_0 - \!\!-\lambda_1' \rightarrow 4d5p\ {}^1P_1 - \lambda_2' \rightarrow [5p_{1/2,3/2}nl_j]_{J=0,1,2}$. The higher lying states, close to the $5p_{1/2}$ threshold, were excited using mainly ICE, according to the scheme $5s^2\,{}^1S_0 - \lambda_1 \rightarrow 5sn'p\,{}^1P_1 - \lambda_2 \rightarrow [5p_{3/2}np_j]_{J=0,1,2}$ with $12 \leq n' \leq 16$. Applying both techniques made possible the recording of the $[5pnp]_{J=0,1,2}$ resonances from $n = 7$ to $n \sim 35$. A description of the experimental set-up and procedure is presented in Section 2.

The calculation used for the theoretical analysis of both valence and ICE spectra involved a combination of the R-matrix method and MQDT, denoted in the following as R-matrix/MQDT method [1]. The main steps of the theoretical calculations are described in Section 3, while Section 4 is devoted to a discussion and analysis of the experimental results.

2 Experiment

2.1 The excitation schemes and the choice of intermediate states

The two different two-step excitation schemes used for the recording of the even $5pnp$ levels of Sr are shown schematically in Figure 1. Scheme (II) refers to the photoionization through the bound state located at 41 172.15 cm^{-1}, which is identified as the $4d5p\ {}^1P_1$ one. This state perturbs strongly the lowest members of the $5sn'p\ {}^1P_1$ series (near $n' \sim 7-8$) and corresponds to the level having the largest amount, about 15−17%, of $4d5p$ character [14] Scheme (I) refers to the ICE method *via* the $5sn'p\ {}^1P_1$ intermediate Rydberg states.

The two-step photoionization ("valence") excitation path (II), $5s^2\ {}^1S_0 - \lambda_1' \rightarrow\ 4d5p\ {}^1P_1 - \lambda_2' \rightarrow [5p_{1/2,3/2}nl_j]_{J=0,1,2}$, was employed mainly for the study of the lower lying $[5pnp]_{J=0,1,2}$ members (roughly for $6 \leq n \leq 10$). The particular intermediate state was chosen because of the expected large oscillator strength for the transitions to both $5pnp$ and $5pnf$ configurations. Moreover, this is the same intermediate state used for the previous study of the $[4dnl]_{J=0,1,2}$ series perturbed by the $[5p6p]_J$ manifold [4,5], so the present recordings constitute, in a way, a continuation of that work. On the other hand this scheme suffers from a number of inconveniences. One of them is the fast decay of the $4d5p\ {}^1P_1$ intermediate state, which has a radiative lifetime of $\tau = 23.4$ ns, and decays mostly to the $4d5s\ {}^1D_2$ state [15]. The latter is photoionized producing thus a large parasitic background. In the previous work [4,5] this was not a major problem, because the λ_2'-excitation wavelengths (see Fig. 1 (II)) were long enough to give rise to a number of sharp and easily identifiable resonances, due to transitions to higher bound states and their subsequent photoionization. In our case however, the wavelengths for the second step were much shorter and could directly photoionize the population accumulated in the $4d5s\ {}^1D_2$ state. The parasitic background created by this mechanism was in many cases structured due to the presence of a number of, usually broad, autoionizing resonances of odd symmetry. One way of avoiding this background would be to collect low energy electrons instead of ions, as was done in previous experiments in Ba [10]. It was found though that this signal did not depend on the polarization of the two lasers. That was manifested in a number of recordings performed with an increased delay (more than 1 μs) between the λ_1' and λ_2' laser pulses, in order to depopulate practically the $4d5p\ {}^1P_1$ state. Thus, the background does not lead to any misinterpretation of the spectra as far as resonant positions, widths and J identification are concerned.

Another worth mentioning point about the valence spectra is the generally very low intensity of the higher $5pnp\ J = 1$ resonances converging to the $5p_{1/2}$ limit. Although this behavior has not been fully understood, it led, on the other hand, to an easy identification of the $J = 2$ lines and helped the clarification of some points in our analysis. However, it became clear that in order to study the full $5pnp$ configuration (except the $J = 3$ series) the ICE technique had to be used. It was actually applied for the study of the high lying $[5p_jnp_{j'}]_{J=0,1,2}$ members through the scheme shown in Figure 1 (I). The ICE recordings were limited to intermediate states with $12 \leq n' \leq 16$ because for $n' < 12$ the $5sn'p$ members present a non-negligible $4d5p$ character while for $n' > 16$ the necessary laser wavelengths for their excitation were not available. Due to the upper limit on n', high lying $[5p_{1/2}np_j]_{J=0,1,2}$ members with $n > 16$ could be observed, because of their mixing with the $[5p_{3/2}np_j]_{J=0,1,2}$ series. This imposed the use of the $5s_{1/2} \rightarrow 5p_{3/2}$ core excitation instead of the $5s_{1/2} \rightarrow 5p_{1/2}$ one. Furthermore, using the "Power-spectrum" technique, it was possible to observe the $[5p_{1/2}np_j]_J$ resonances for $11 \leq n \sim 35$. These states are perturbed by the $[5p_{3/2}np_j]_J$ resonances lying below the $5p_{1/2}$ limit for $n \leq 14$, giving thus rise to a number of apparently complex structures. Finally, above the $5p_{1/2}$ limit the profiles of the $5p_{3/2}np_j$ $(n > 14)$ resonances are strongly modified by the ICE envelope zeros. Hence, it was necessary to refer again to the valence spectra for the calibration of these resonances.

2.2 Experimental set-up and procedure

The two-step photoionization method was applied in the National Research Center Lab, in Athens, and the details of the experimental set-up have been given elsewhere [5]. Briefly, an effusive Sr atomic beam was crossed at right angles by two laser beams. The first excitation step was achieved with 100 μJ light pulses of $\sim$ 5 ns duration, produced from a Nd-YAG pumped dye laser (Datachrom, Quantel) and frequency doubled ($\lambda_1' \approx 242.8$ nm) with an LFM doubling crystal (Quantum Technology). The second excitation step (λ_2', in the range 510−343 nm) was achieved with 8 ns, 10 μJ light pulses from a XeCl excimer pumped dye laser (Lumonics, ED-300). The produced Sr^+ ions were selected by a pulsed TOF arrangement and detected by a tandem multichannel plate detector. The detector signal was further processed by a Boxcar integrator and fed to both a recorder and a PC unit.

The ICE technique was applied at the Atomic and Molecular Physics Lab, in Ioannina, and the experimental set-up was very similar to that used for the study of the $[4pnp]_J$ states of Ca [13]. In this experiment an effusive Sr atomic beam was first excited to a bound $5sn'p\ {}^1P_1$ Rydberg state by the light pulses of a homemade oscillator-amplifier dye laser. The latter was pumped by a portion of the output of a XeCl (QUESTEK 2000) laser. The dye laser output was frequency doubled, resulting in pulses of a few μJ and $\sim$ 10 ns duration (λ_1, lying in the range of 223.8−220.6 nm). For the second step the $\sim$ 5 ns output of a Lambda Physik (LPD 3000) dye laser pumped by the same XeCl laser was used ($\lambda_2 \approx 407.8$ nm). The energy of the pulses for this second excitation step could be reduced down to a few μJ with neutral density filters, in order to avoid signal saturation effects while saturated spectra were recorded with the full power of the laser beam (a few hundred μJ).

The Sr^+ ions were extracted by a DC voltage of $\sim$ 100 V and, after passing through a $\sim$ 10 cm field free region, they were detected by a channeltron detector (Galileo 4870). The electrical signal was processed through a gated integrator (Stanford Research Systems SR250) and a chart recorder (Yukogawa LR4120) connected to a PC computer.

In both, Athens and Ioannina, experiments the dye lasers used for the second excitation step had a bandwidth of $\sim$ 0.2 cm^{-1}. Their frequency calibration was achieved by the simultaneous recording of the optogalvanic signal from a commercial Ar hollow-cathode lamp, interacting with a small ($\sim$ 2%) portion of the λ_2 (or λ_2')

laser beam, and the interference fringes produced on another small portion of the same laser beam upon its transmission through an evacuated Fabry-Perot interferometer of FSR = 1.00 cm^{-1} (Athens) or 1.841 cm^{-1} (Ioannina). Both excitation steps were performed with linearly polarized light and the polarization for the second step could be rotated by means of a double Fresnel rhomb. In this way the polarization of the two laser beams could be set either parallel or perpendicular to each other. When both beams have parallel polarizations ($\pi\pi$), the $J = 0$, 2 $5pnp$ states can be reached, while with mutually perpendicular polarizations ($\pi\sigma$) states with $J = 1$, 2 can be excited [5,13].

3 Theoretical calculations

The experimental data are analyzed by making use of the jj-coupled eigenchannel R-matrix/MQDT method [1]. Only some basic points of the approach relevant to the discussion of this paper will be outlined below.

In the jj-coupled eigenchannel R-matrix approach, the wavefunctions describing the valence electrons outside a frozen Sr^{2+} core are determined variationally within a spherical reaction volume of radius r_0 for given energy values. It is assumed that only one electron can escape from the reaction volume and that beyond r_0 the escaping electron moves in a pure Coulomb potential. The variational R-matrix calculation gives the logarithmic derivative of the wavefunctions, with fixed J, E and parity π, at the surface of the reaction volume. Outside the reaction volume, the R-matrix eigenstates are matched to Coulomb expansions giving a short-range reaction matrix $K_J(E)$ which depends smoothly on energy and refers to the MQDT fragmentation channels. As described in an earlier paper dealing with the homologous $4pnp$ even-parity autoionizing Rydberg series of Ca with $J = 0$, 1 and 2 [13], the short-range reaction matrices K_J include 5, 13 and 17 interacting channels respectively, which in the case of Sr consist of the open channels $Nl_j\varepsilon l'_{j'}$ converging to the $Nl_j \equiv 5s$, $4d_j$ thresholds and the closed channels $Nl_jnl'_{j'}$ ($l' \leq 4$) converging to the $Nl_j \equiv 5p_j$ thresholds. MQDT is used to extend the wave functions to distances larger than the R-matrix reaction volume. The eigenchannel MQDT formulation [16] or the phase-shifted MQDT formulation [17, 18] is used to impose boundary conditions at large r and to calculate the observables.

In the autoionizing energy range, the number of physical solutions equals the number of the open channels N_0. The asymptotic form of the collision eigenchannel function satisfying standing wave boundary conditions, is given by:

$$\Psi_\rho(E) = \Sigma_{i'\in o}\phi_{i'}T_{i'\rho}(E) + \Sigma_{i\in c}\,\phi_i\,Z_{i\rho}(E) \qquad (1)$$

where ($i' \in o$) and ($i \in c$) denote the open and closed channels and the coefficients $T_{i'\rho}(E)$ and $Z_{i\rho}(E)$ describe the relative admixture of the open $\phi_{i'}$ and closed ϕ_i fragmentation channels respectively.

The theoretical spectra presented in this paper concern only the isolated-core excitation scheme $5s^2 \rightarrow 5sn'p\ ^1\mathrm{P}_1 \rightarrow 5pnp$ $J = 0{-}2$. The R-matrix calculations were performed using a reaction volume of radius $r_0 =$ 20 a.u. The photoionization cross-sections were calculated in the ICE approximation [19]. This approximation assumes a negligible excitation of the open channels i', while among the closed channels i, only the $i \equiv 5p_{1/2,3/2}np_j$ ones are excited and the corresponding dipole matrix elements D_i are given by the product of the transition moment $5s_{1/2} \rightarrow 5p_j$ of the inner electron with the overlap integral of the outer electron [20]. The energy-dependent overlap integral was calculated analytically and exhibits a strong central lobe near $E_0 + \Delta_j$, where E_0 corresponds to the energy of the initial $5sn'p\ ^1\mathrm{P}_1$ level and Δ_j to the energy of the ionic transition $5s \rightarrow 5p_j$, and much weaker secondary lobes periodic in ν_j (ν_j is the effective quantum number with respect to the $5p_j$ threshold) and separated by zeros. In order to observe structures within the satellite lobes, ICE spectra were recorded by saturating the central lobe [9]. To account for saturation effects, the spectra were calculated from the unsaturated spectra $\sigma(E)$ using the relation

$$\sigma_{\mathrm{S}}(E) = A\{1 - \exp(-S\sigma(E)/\sigma_{\mathrm{m}})\}, \qquad (2)$$

where σ_{m} is the maximum cross-section. The scaling factor A and the saturation parameter S are fitted to the experimental data.

For unpolarized light, the photoionization cross-section is proportional to

$$\Sigma_\rho|\Sigma_i Z_{i\rho}D_i|^2. \qquad (3)$$

It is well-known that low members of the $5sn'p\ ^1\mathrm{P}_1$ Rydberg series of Sr are interacting with the $4d5p\ ^1\mathrm{P}_1$ level. However, for $n' > 12$, the $5sn'p{-}4dnp$ mixing is very small [14,21] and can be neglected. Thus, the dipole matrix elements D_i were calculated by assuming that the wavefunctions $|\Psi_{n'}\rangle$ of the initial $5sn'p$ levels can be written as $|\Psi_{n'}\rangle = \alpha_{n'}|5sn'p\ ^1\mathrm{P}_1\rangle + \beta_{n'}|5sn'p\ ^3\mathrm{P}_1\rangle$, where we use values previously obtained [21] for the mixing coefficients $\alpha_{n'}$ and $\beta_{n'}$. Cross-sections for mutually parallel or perpendicular laser polarization are given by:

$$\sigma_\parallel = \frac{1}{3}\sigma_{J=0} + \frac{2}{15}\sigma_{J=2} \quad \text{and} \quad \sigma_\perp = \frac{1}{12}\sigma_{J=1} + \frac{1}{20}\sigma_{J=2} \qquad (4)$$

where σ_J denotes the excitation cross-sections with unpolarized light of levels with a given J.

The assignment of the observed levels and the general trends along the $5p_j\,np_{j'}$ Rydberg series can be obtained by applying MQDT techniques, developed for bound states, to effective reaction matrices $K_{\mathrm{eff},J}$ which, for each J-value, are defined as the real part of κ_{cc}, given by

$$\kappa_{cc} = K_{cc} - K_{co}(\mathrm{i}I_{oo} + K_{oo})^{-1}K_{oc} \qquad (5)$$

and expressing the restriction of the K_J-matrix to the space (c) of the closed channels [1,16,18]. The $K_{\mathrm{eff},J}$ reaction matrix can be used to determine the positions of the resonances and to identify them by calculating for

each level the coefficients $Z_i^{(n)}$ of the decomposition of the wavefunctions on the closed channels i. The assignments obtained in this way for $J = 0-2$ levels located below the $5p_{1/2}$ threshold will be reported later in Tables 2 to 4. The interaction among closed channels will be analyzed graphically using Lu-Fano plots [16]. Note, however, that such a procedure is adequate to locate the position of a resonance with an error comparable to its autoionization width and that it is not suitable to analyze the very broad autoionizing resonances, in particular the $5pnf$ ones.

Quantitative information on the resonance energies, widths and assignments of the autoionizing levels, independent of the excitation scheme, can also be obtained [1] by analyzing the energy dependence of the partial densities of states in the closed channels i:

$$ds_i(E) = \Sigma_\rho [Z_{i\rho}(E)]^2. \quad (6)$$

We have systematically compared the assignments of the resonances obtained from partial densities of states to those calculated from the effective reaction matrices restricted to closed channels. Differences occur only in a few cases (see Tab. 3).

We have also attempted to calculate the photoionization spectra observed using the two-step excitation scheme *via* the $4d5p\ ^1P_1$ valence state. The calculation requires, in addition to the short-range reaction matrices describing final states, the dipole matrix elements connecting the R-matrix eigenstates to the $4d5p\ ^1P_1$ valence state. These matrix elements are computed within the reaction volume and the initial and final states must be determined within the same reaction volume. As in a previous paper dealing with the same excitation scheme in the energy range below the $4d_{5/2}$ threshold [5] calculations were performed using a reaction volume of radius $r_0 = 35$ a.u. However, above the $4d_{5/2}$ threshold, theoretical spectra are in poor agreement with the observed ones. This suggests that the reaction volume is not large enough for an adequate description of the $4d5p\ ^1P_1$ valence state, which is mixed indeed with $5sn'p$ Rydberg states. We have not attempted to improve the description of the valence state using a larger reaction volume and thus theoretical spectra corresponding to the excitation scheme *via* the $4d5p\ ^1P_1$ state will not be presented in this paper.

Phase-shifted MQDT parameters can be calculated by using the formulation worked out by Lecomte [18]. This formulation starts from the complex reaction matrix $\kappa_{cc'}$ given in equation (5). Defining closed fragmentation channels on phase-shifted Coulomb functions, leads to phase-shifted quantum defects μ_i and to a transformed complex reaction matrix κ_{cc}, with elements of the form $\kappa_{ij} = r_{ij} + \mathrm{i}\mathbf{R}_i \cdot \mathbf{R}_j$. The symmetric and real matrix r_{ij}, with $r_{ii} = 0$, describes the direct coupling between the closed channels and the N_c vectors $\mathbf{R}_i$ describe the couplings between the closed channels and the continua. When the resonances pertaining to channel i are well separated from the others, μ_i and $|\mathbf{R}_i|^2$ characterize the positions and scaled autoionizing widths $\gamma_i \equiv \Gamma_i(\nu_i)^3 = 2|\mathbf{R}_i|^2/\pi$ (Γ_i is the FWHM autoionization width in a.u. and ν_i is the effective quantum number). Such a procedure was used to analyze the positions and widths of the resonances located above the $5p_{1/2}$ threshold.

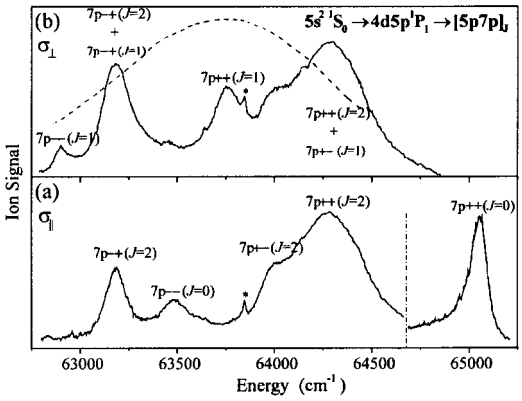

Fig. 2. The $[5p7p]_{J=0,1,2}$ multiplet as recorded through the $4d5p\ ^1P_1$ intermediate state with (a) parallel ($\sigma_\parallel$) and (b) perpendicular ($\sigma_\perp$) mutual polarization of the two laser beams. The dashed line is the dye profile. The vertical dashed-doted line denotes that the $[5p_{3/2}7p_{3/2}]_{J=0}$ line is recorded in a separate scan with different sensitivity. The line marked with an asterisk is a parasitic one.

4 Results and discussion

4.1 Excitation cross-sections

Figure 2 shows a part of the spectrum recorded through the valence $4d5p\ ^1P_1$ intermediate state using parallel and perpendicular linear polarizations. The structures correspond to the $[5p7p]_J$ multiplet. The J-assignment for the excited states is obtained by comparing the energy positions of the resonances observed in the two recordings. The resonances are easily identified, because the superposition of different J resonances just above the $4d_{5/2}$ threshold is not as substantial as for the high lying $[5pnp]_J$ members. Based on the theoretically predicted energy level positions we have marked the two unobserved resonances, namely the $[5p_{1/2}7p_{3/2}]_{J=1}$ and $[5p_{3/2}7p_{1/2}]_{J=1}$ ones, despite the fact that they are blended with $J = 2$ lines. The resonance marked with an asterisk is a parasitic one. By applying a long delay between the λ_1' and λ_2' laser pulses it is made evident that it originates from the direct photoionization of the $5s4d\ ^1D_2$ level, populated from the decay of the $4d5p\ ^1P_1$ state (see Sect. 2.1).

The analysis of the experimental ICE spectra concerning the high lying members of the $[5pnp]_J$ series was greatly facilitated from the comparison with the corresponding theoretical cross-sections. It is to be emphasized that the method of assigning J-values to the resonances through a comparison of spectra obtained using different linear laser polarization combinations can be applied either for the theoretical or the experimental spectra. This procedure is illustrated in Figure 3, which displays the calculated cross-sections from the initial $5s13p$ Rydberg state using both polarization schemes. The energy-dependence

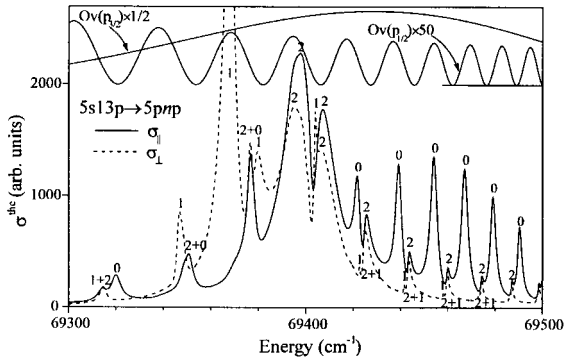

Fig. 3. Theoretically calculated ICE cross-sections through the $5s13p$ bound Rydberg state using mutually parallel ($\sigma_\parallel$) and perpendicular ($\sigma_\perp$) light polarization combinations. On the top of the graph it is also shown the energy dependence of the squares of the overlap integrals associated with the ionic transitions $5s_{1/2} \rightarrow 5p_{1/2}$ (Ov($p_{1/2}$)) and $5s_{1/2} \rightarrow 5p_{3/2}$ (Ov($p_{3/2}$)).

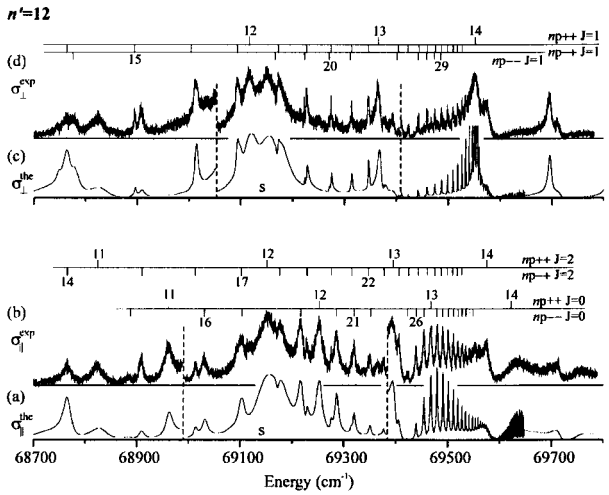

Fig. 4. ICE cross-sections corresponding to the excitation from the $5s12p\ ^1P_1$ intermediate state. (a) Theoretical $\sigma_\parallel$, (b) experimental $\sigma_\parallel$ (c) theoretical $\sigma_\perp$ and (d) experimental $\sigma_\perp$ cross-section. The vertical dashed lines separate energy ranges recorded with different pulse energies of the λ_2-exciting laser. Saturation effects affect the central part of the experimental cross-sections (denoted by S). Such effects have been also introduced in the corresponding theoretical cross-sections using equation (2). On the top of each experimental spectrum they are shown the level assignments for each J value, as calculated by theory.

for the squares of the overlap integrals associated with the ionic transitions $5s_{1/2} \rightarrow 5p_{1/2}$ and $5s_{1/2} \rightarrow 5p_{3/2}$ are also reported. The λ_2 laser light is approximately resonant with the $5s_{1/2} \rightarrow 5p_{3/2}$ ionic transition and the calculated energy-range covers in this case the very intense and broad central lobe of the overlap integral of the $5s_{1/2}$ and $5p_{3/2}$ orbitals. On the other hand only weak and narrow secondary lobes are observed for the overlap integral of the non-resonant ionic transition $5s_{1/2} \rightarrow 5p_{1/2}$, with a periodicity $\Delta\nu_{1/2} = 1$ in the effective quantum number of the $5p_{1/2}np_j$ channels. The more intense structure of each spectrum, near 69 395 cm^{-1} and 69 360 cm^{-1} for the $\sigma_\parallel$ and $\sigma_\perp$ cross-sections respectively, is ascribed to $[5p_{3/2}13p_j]_J$ resonances, which are predominantly excited, because of the specific choice of the $5s_{1/2} \rightarrow 5p_{3/2}$ core excitation.

In accordance with equation (4) we can ascribe to $J = 2$ the resonance structures appearing in both, $\sigma_\parallel$ and $\sigma_\perp$, cross-section spectra. The additional resonances observed in the $\sigma_\parallel$ ($\sigma_\perp$) spectra only are identified as $J = 0$ ($J = 1$). The labeling with an additional J of an observed structure can be obtained through the theoretical decomposition of each of the $\sigma_\parallel$ and $\sigma_\perp$ spectra to their σ_J contributions. Examination of the theoretical intensities shows that the levels identified this way correspond either to blended resonances or to resonances that are stronger than the already identified ones. A more precise identification, concerning especially the distinction between $[5p_{1/2}np_{1/2}]_{J=1}$ and $[5p_{1/2}np_{3/2}]_{J=1}$ structures, which are not always resolved, is achieved by comparing the profiles calculated for the cross-section to the profiles associated with the two partial densities of states ds_i, where $i \equiv 5p_{1/2}np_j$ $J = 1$ and $j = 1/2$, $3/2$ (Eq. (6)). Finally, energy level positions and their assignment are confirmed by the results obtained from the $K_{\mathrm{eff},J}$ matrices.

The comparison of the experimental spectra to the theoretical ones shows clearly that the recorded spectra suffer from a substantial superposition of resonances having different J values. Another point to mention is that some lines, which show up in some spectra corresponding to particular $5sn'p\ ^1P_1$ lower levels, are masked in the spectra through different $5sn'p\ ^1P_1$ levels. One characteristic example concerns the $J = 1$ resonance around 69 400 cm^{-1} which appears as a well resolved structure in the recorded spectra for $n' = 14$ and 15, while it is masked for the $n' = 12$ and 13 ones.

As in the ICE spectra, in the recorded spectra through the excitation of the $4d5p\ ^1P_1$ valence state, levels having a dominant $[5p_{1/2}np_j]_J$ character and being far from the $[5p_{3/2}np_j]_J$ perturbers are relatively weakly excited. This can be attributed to a qualitatively different reason, which has to do with the fact that in the wave function of the intermediate $4d5p\ ^1P_1$ level the components $4d_j5p_{3/2}$ prevail, favoring the excitation of the $[5p_{3/2}np_j]_J$ channels. Furthermore, in the latter spectra direct excitation of the closed $[4f_{5/2}np_j]_J$ channels and of the continuum is possible. The comparison of the ICE spectra with the valence ones is very useful to confirm the identifications, especially below the $5p_{1/2}$ limit, where the $J = 1$ series are very weakly excited. Thus the identification and calibration of the $J = 2$ resonances becomes easier in the valence spectra and the problems associated with the superposition between $J = 1$ and $J = 2$ lines are avoided.

The ICE spectra through the first step excitation of the $5s12p$ and $5s14p$ levels are presented in Figures 4 and 5. The experimental spectra as well as the theoretical ones, obtained using parallel and perpendicular laser polarizations, are reported. The central parts of the spectra correspond to the central lobe of the resonant ionic

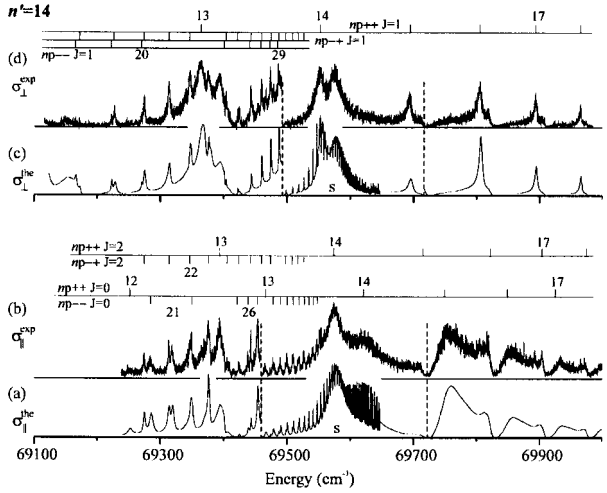

Fig. 5. Same as in Figure 4 but for the $5s14p\ ^1\mathrm{P}_1$ intermediate state.

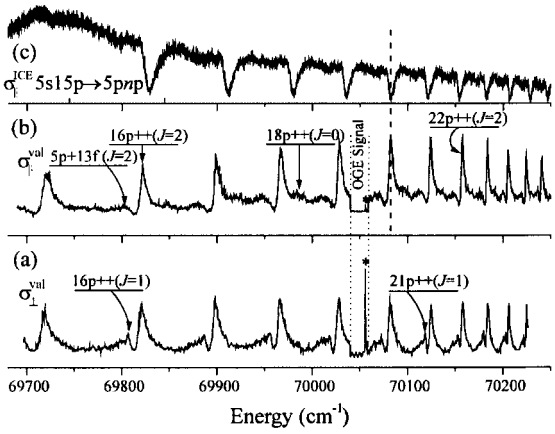

Fig. 6. (a and b) Valence spectra above the $5p_{1/2}$ ionization limit recorded through the $4d5p\ ^1\mathrm{P}_1$ intermediate state with mutually perpendicular ($\sigma_\perp$) and parallel ($\sigma_\parallel$) laser polarizations respectively. (c) ICE spectrum above the $5p_{1/2}$ limit recorded through the $5s15p\ ^1\mathrm{P}_1$ intermediate state with parallel laser polarizations. The vertical dashed line shows that the maxima of the $[5p_{3/2}np_{3/2}]_{J=2}$ (np^{++}) lines are very close to the ICE overlap integral zeros. A part of the optogalvanic (OGE) wavelength calibration spectrum is also shown.

transition $5s_{1/2} \rightarrow 5p_{3/2}$ and in these energy-ranges, the experimental intensities have been divided by a factor of about 10 to 100, while saturation effects, denoted by S, have been introduced in the theoretical cross-sections. The doubly-excited levels, identified experimentally in the present study and classified as belonging to the $[5p_{j'}np_j]_J$ series, are indicated in the figures using the notation $np\pm\pm J$. The energy-positions, autoionization widths and identifications of the corresponding structures are given in Tables 2–4. No discontinuity is observed in the experimental spectra at the energy of the Sr^+ $5p_{1/2}$ ionization threshold (69 647.38 cm^{-1}), where the highest members of the $[5p_{1/2}np_{1/2,3/2}]_J$ series are not resolved but they are diluted in the broad structures associated with the $[5p_{3/2}14p_{1/2,3/2}]_J$ perturbers. On the contrary the limit of the $[5p_{1/2}np_{1/2,3/2}]_J$ series is quite visible on the theoretical spectra. The energy-ranges corresponding to a negligible absorption correspond to the zeros of the $5s_{1/2} \rightarrow 5p_{3/2}$ overlap integral, especially evident above the $5p_{1/2}$ threshold. For example in the $n' = 14$ spectrum, these zeros occur near 69 200, 69 420, 69 720, 69 830, 69 910 cm^{-1}. The energies of these zeros depend on the n'-value of the intermediate state, which demonstrates the need of studying the "Power-spectrum" for different intermediate states. The agreement between experimental and theoretical spectra emphasizes the efficiency of the R-matrix/MQDT method to analyze doubly excited states lying below the low-lying ionization thresholds in alkaline-earth atoms.

The valence spectra recorded in the energy-range above the $5p_{1/2}$ ionization limit for both polarization schemes are compared, in Figure 6, to the ICE spectrum from the intermediate $5s15p$ level with parallel polarizations. This comparison illustrates the differences in the spectra obtained using quite different excitation schemes. The $5p_{3/2}np_{3/2}$ $J = 1,\ 2$ resonances show asymmetrical profiles in the valence spectra, which demonstrates that closed as well as open channels are excited by using a valence state as an intermediate state in the excitation process. Furthermore, because of $4dnf$ configuration-mixing in the wave function of the $4d5p\ ^1\mathrm{P}_1$ intermediate level, $5p_{3/2}nf_J$ $J = 2$ states appear as broad and weakly excited resonances in the valence spectra. In the ICE spectra, the most visible features are ascribed to the zeros in the $5s_{1/2} \rightarrow 5p_{3/2}$ overlap integral which modify strongly the resonance structure of the observed cross-section. The σ_J, $J = 0,\ 2$, contributions to the total theoretical cross-section demonstrate that the $5p_{3/2}np_{3/2}$ $J = 0$ resonances occur near the maxima of the overlap integral, while the profiles of the $5p_{3/2}np_{3/2}$ $J = 2$ ones, located near the low energy-side of the zeros, are strongly modified by the energy-dependence of the overlap integral.

4.2 Level structure above the $5p_{1/2}$ threshold

Above the $5p_{1/2}$ limit, there are eight different series with $J = 0{-}2$ converging to the $5p_{3/2}$ threshold, two $J = 2$, two $J = 1$ and one $J = 0$ $5pnp$ series and two $J = 2$ and one $J = 1$ $5pnf$ series. The experimental ICE spectra show three series. From the comparison between $\pi\pi$ and $\pi\sigma$ spectra (Figs. 4 and 5) the most clearly identified series are one with $J = 0$ ($5p_{3/2}np_{3/2}$) and one with $J = 1$. Additionally, a $J = 2$ series is observed, the apparent maxima of which are located very close to the successive zeros of the ICE overlap integrals (Fig. 6). We should recall here that the study of this part of the spectrum using ICE had to rely on the "Power-spectrum" technique, because the available wavelengths for the excitation of the Rydberg $5sn'p$ intermediate states with $n' > 16$ were not available. The difficulties stemming from profile deformations are tackled by invoking the valence spectra, recorded through the $4d5p\ ^1\mathrm{P}_1$ state. As seen in Figure 6,

Table 1. Observed Rydberg series, their quantum defects μ and their scaled widths $\Gamma\nu^3$ above the $5p_{1/2}$ ionization threshold compared to theoretical values deduced from the phase-shifted MQDT formalism. The ICE measurements are reported for the observed $J = 1$ levels which are in agreement with the valence spectra measurements made through the $4d5p\ ^1\mathrm{P}_1$ intermediate state. For all the other series the data refer to the valence spectra either because they are absent from the ICE spectra ($[5p_{3/2}nf_j]$) or because their lineshapes are deformed near the ICE overlap integral zeros ($5p_{3/2}np_{3/2}$, $J = 0$ and 2).

			μ		$\Gamma\nu^3$ ($\times 10^3$ cm^{-1})	
Rydberg Serie	J	Range	Exp.	Th.	Exp.	Th.
$5p_{3/2}np_{3/2}$	0	$15 \le n \le 21$	2.47 ± 0.05	2.46	64.6 ± 5.2	72.4
$5p_{3/2}np_{3/2}$	1	$15 \le n \le 30$	2.94 ± 0.02	2.93	16.9 ± 0.6	11.8
$5p_{3/2}np_{3/2}$	2	$15 \le n \le 28$	2.78 ± 0.05	2.78	20.5 ± 0.8	28.7
$5p_{3/2}nf_j$	2	$13 \le n \le 24$	0.05 ± 0.02	0.10	53.3 ± 2.5	–

these spectra reveal two $J = 2$ series and the level positions of the strongest $J = 2$ series, ascribed to the unresolved $5p_{3/2}np_{1/2}$ and $5p_{3/2}np_{3/2}$ states are located near the ICE overlap integral zeros. Therefore the $J = 2$ resonances are strongly deformed due to the overlap integral variation and their apparent maxima do not correspond to their true positions (see Sect. 2). Consequently, it was found necessary to determine their energies and widths using the valence spectra. The other broad and weakly excited $J = 2$ series, having very small quantum defects $\mu(\mathrm{mod}\ 1) \approx 0.05$, is identified as $5p_{3/2}nf_j$. Because of destructive interference effects in the dipole matrix elements, the members of the $5p_{3/2}np_{1/2}$ series, with the theoretically predicted quantum defect $\mu(\mathrm{mod}\ 1) \approx 0.85$ were not observed.

Although recorded in both ICE and valence spectra, it is difficult to calibrate and measure the widths of the $[5p_{3/2}np_{3/2}]_{J=0}$ resonances. They are very broad and the profiles are slightly deformed by the overlap integral zeros in the ICE spectra. The quantum defect $\mu(\mathrm{mod}\ 1) \approx 0.46$ measured from the energy-dependence of the density of states agrees with the value $\mu(\mathrm{mod}\ 1) \approx 0.45$ obtained by a parametric MQDT analysis of levels lying below the $5p_{1/2}$ limit and excited through the $4d5p\ ^1\mathrm{P}_1$ intermediate level [22]. Because of the deformation due to the overlap integral, these values differ noticeably from the values $\mu(\mathrm{mod}\ 1) \approx 0.35$, deduced from the maxima in the theoretical ICE spectra, and $\mu(\mathrm{mod}\ 1) = 0.39 \pm 0.05$, measured from the experimental ICE spectra above the $5p_{1/2}$ threshold. On the other hand, only a few members are comfortably measured in the valence spectra because, apart of their large widths, they are weakly excited and partially superimposed with the $[5p_{3/2}np_{3/2}]_{J=2}$ lines. Nevertheless, we report the valence spectra measurements in Table 1. The quantum defect $\mu(\mathrm{mod}\ 1) \approx 0.47$ in this case agrees with the value obtained from the density of states analysis but differs from the one obtained from the ICE profiles.

The $J = 1$ levels recorded in the ICE spectra do not suffer significantly from modifications due to the overlap integral, since their energy positions are close to the maxima of the secondary lobes of the overlap integral and their widths are much narrower than the lobe widths. Indeed, the theoretically computed cross-sections reveal lineshapes that agree with those calculated from the density of states ds_i for $i \equiv 5p_{3/2}np_{3/2}$. However, only one $J = 1$ series was observed and is identified as the $5p_{3/2}np_{3/2}$ one. Its measured constant quantum defect and scaled ionization width, given in Table 1, are in good agreement with the theoretical values obtained from the phase-shifted MQDT parameters. Concerning the $[5p_{3/2}np_{1/2}]_{J=1}$ series, with a theoretical quantum defect $\mu(\mathrm{mod}\ 1) \approx 0.79$, a comparison between the theoretical cross-sections and the density of states demonstrates that, because of interference effects in the transition matrix element, it can not be excited through the ICE scheme.

The experimentally determined quantum defects and scaled widths for all the observed series are assembled in Table 1. For the $5pnp$ series the agreement is quite good, within the given uncertainties, with the theoretical values obtained using the phase-shifted MQDT formulation. The observation in Sr of only one $J = 1$ and two $J = 2$ series above the $5p_{1/2}$ threshold can be compared to the corresponding ICE spectra in Ca and Ba. In Ca, the $[4p_{3/2}np_{1/2}]_{J=1,2}$ series cannot be excited from the $4pn'p\ ^1\mathrm{P}_1$ LS-coupled intermediate levels [13]. In Ba, the $[6p_{3/2}np_{1/2}]_{J=1}$ series was found to be hardly resolved from the strongest $[6p_{3/2}np_{3/2}]_{J=2}$ resonances [11] while photoionization spectra corresponding to the second step excitation $5d6p\ ^3\mathrm{P}_0 \rightarrow J = 1$ and $5d6p\ ^3\mathrm{P}_1 \rightarrow J = 2$ have been investigated experimentally [23] and theoretically [12] only below the $6p_{1/2}$ threshold. The $6pnp$ and $6pnf$ levels were also investigated through selected $5d6p$ $J = 0{-}4$ levels [24]. All these studies have shown that, as observed in the valence spectra of Sr, the $6pnf$ autoionizing series exhibit broad structures with much broader widths than the $6pnp$ series.

4.3 Level structure below the $5p_{1/2}$ threshold

The experimentally measured energy level positions (resonant maxima) and widths, together with theoretical energies and identifications for the $5pnp$ states, below the $5p_{1/2}$ ionization threshold, are assembled in Tables 2, 3 and 4 for $J = 0$, 1 and 2 respectively. The uncertainty of the reported linewidths is $\sim 10\%$ while for each energy-position

Table 2. $5pnp\ J = 0$ series below the $5p_{1/2}$ Sr limit.

	Experiment			Theory	
Energy (cm^{-1})	Width (cm^{-1})	$\nu_{1/2}$	$\nu_{3/2}$	Energy (cm^{-1})	Assignment
[a]61 971	250	3.781	3.598	62 039.0	$5p + 6p+$
[a]63 459	78	4.211	3.962	63 534.6	$5p - 7p-$
[a]65 041	102	4.881	4.505	65 072.0	$5p + 7p+$
[a]65 761	66	5.314	4.838	65 785.8	$5p - 8p-$
[a]66 644	53	6.045	5.370	66 639.6	$5p - 9p-$
[a]67 045	46	6.507	5.687	67 066.6	$5p + 8p+$
(b $J = 2$)		[c]*7.177*	[c]*6.118*	67 517.1	$5p - 10p-$
[a]67 852	33	7.818	6.501	67 869.5	$5p + 9p+$
[a]68 078	26	8.362	6.803	68 079.2	$5p - 11p-$
(b $J = 2$)		*9.139*	*7.203*	68 333.5	$5p - 12p-$
[a]68 510	19	9.823	7.523	68 513.0	$5p + 10p+$
[a]68 626	13	10.365	7.759	68 632.0	$5p - 13p-$
(b $J = 2$)		*11.193*	*8.088*	68 771.5	$5p - 14p-$
68 887	7.3	12.013	8.382	68 888.0	$5p - 15p-$
68 961	13	12.644	8.588	68 964.9	$5p + 11p+$
69 030	11	13.332	8.794	69 032.7	$5p - 16p-$
69 103 ($+J = 2$)	< 9	14.198	9.030	69 104.6	$5p - 17p-$
(b $J = 2$)		*15.114*	*9.252*	69 167.0	$5p - 18p-$
69 216	< 6.5	15.949	9.435	69 216.8	$5p - 19p-$
69 252	< 9	16.660	9.575	69 254.2	$5p + 12p+$
69 285	7.5	17.402	9.710	69 287.1	$5p - 20p-$
69 319.1	4	18.283	9.856	69 320.2	$5p - 21p-$
69 350.7($+J = 2$)	3	19.232	9.996	69 350.8	$5p - 22p-$
(b $J = 2$)		*20.180*	*5.978*	69 377.9	$5p - 23p-$
(b $J = 2$)		*21.122*	*10.236*	69 401.4	$5p - 24p-$
69 421.8	1.7	22.056	10.337	69 421.9	$5p - 25p-$
69 438.9	2.5	22.943	10.424	69 439.5	$5p - 26p-$
69 453.8	3	23.809	10.502	69 454.6	$5p - 27p-$
69 466.8	3.9	24.651	10.571	69 467.8	$5p + 13p+$
69 478.7	3.3	25.506	10.636	69 479.7	$5p - 28p-$
69 489.9	2.4	26.398	10.697	69 490.8	$5p - 29p-$
69 500.5	2	27.333	10.757	69 501.2	$5p - 30p-$
69 510.4	1.7	28.304	10.814	69 510.8	$5p - 31p-$
69 519.5	1.5	29.294	10.866	69 519.6	$5p - 32p-$
69 527.4	1	30.243	10.913	69 527.7	$5p - 33p-$
69 534.9	≤ 1	31.235	10.958	69 535.0	$5p - 34p-$
69 542.0	≤ 1	32.270	11.000	69 541.8	$5p - 35p-$
69 548.1 ($+J = 2$)	≤ 1	33.246	11.038	69 547.9	$5p - 36p-$
(b $J = 2$)		*34.207*	*11.071*	69 553.6	$5p - 37p-$
(**) 69 621	~ 40	64.497	11.513	(**) 69 623	$5p + 14p+$

[a]: Recorded only through the valence $4d5p\ ^1P_1$ intermediate state. (b $J = 2$): blended with a $J = 2$ resonance. ($+J = 2$): superimposed with a $J = 2$ resonance. **: Maximum of unresolved perturber envelope as observed through the $5s14p\ ^1P_1$ intermediate level with parallel laser polarizations. [c]: For experimentally unobserved energy levels the reported effective quantum numbers are calculated from the theoretical values and are given in italics.

Table 3. $5pnp$ $J = 1$ series below the $5p_{1/2}$ Sr limit.

Experiment				Theory	
Energy (cm^{-1})	Width (cm^{-1})	$\nu_{1/2}$	$\nu_{3/2}$	Energy (cm^{-1})	Assignment
[a]62 897	67	4.032	3.738	62 896.2	$5p-7p-$
(b $J = 2$)		[c]*4.131*	[c]*3.896*	63 211.8	$5p-7p+$
[a]63 740	80	4.310	3.957	63 747.9	$5p+7p+$
(b $J = 2$)		*4.509*	*4.207*	64 190.3	$5p+7p-$
[a]65 339	53	5.047	4.504	65 348.5	$5p-8p-$
(b $J = 2$)		*5.169*	*4.729*	65 522.6	$5p-8p+$
[a]66 137	~ 85	5.591	4.878	66 184.3	$5p+8p+$
		5.807	*5.202*	66 374.1	$5p+8p-$
[a]66 659	25	6.060	5.180	66 676.1	$5p-9p-$
(b $J = 2$)		*6.187*	*5.469*	66 770.4	$5p-9p+$
[a]67 419	11.5	7.017	5.741	67 429.4	$5p+9p+$
		7.108	*6.075*	67 498.5	$5p-10p-$
		7.212	*6.139*	67 526.1	$5p-10p+$
		7.337	*6.216*	67 602.4	$5p+9p-$
[a]67 959	9	8.062	6.272	67 960.5	$5p-11p-$
nr		*8.177*	*6.702*	68 002.5	$5p-11p-$
[a]68 242	12.5	8.836	6.616	68 251.0	$5p+10p+$
nr		*9.092*	*7.180*	68 316.7	$5p-12p-\$$
		9.141	*7.203*	68 329.3	$5p+10p-\$$
(b $J = 2$)		*9.234*	*7.249*	68 358.0	$5p-12p+$
[a]68 564.6	5.5	10.067	7.631	68 565.1	$5p-13p-$
(b $J = 2$)		*10.180*	*7.680*	68 586.6	$5p-13p+$
[a]68 743.7	8	11.047	8.033	68 748.1	$5p-14p-\$$
68 764 ($+J = 2$)	~ 8	11.159	8.076	68 766.2	$5p-14p+\$$
68 775	10	11.216	8.097	68 779.2	$5p+11p-\$$
(b $J = 2$)		*11.506*	*8.204*	68 818.6	$5p+11p+\$$
68 894.7	4	12.075	8.403	68 896.5	$5p-15p-$
		12.184	*8.440*	68 908.2	$5p-15p+$
69 003.9	~ 1	13.152	8.742	69 004.2	$5p-16p-$
		13.168	*8.747*	69 014.5	$5p-16p+$
69 093.5 ($+J = 2$)	7.5	14.076	8.998	69 094.3	$5p-17p-$
		14.182	*9.026*	69 101.7	$5p-17p+$
69 116	12	14.371	9.074	69 120.1	$5p+12p+$
		14.873	*9.196*	69 151.3	$5p+12p-$
69 165.8	~ 2	15.108	9.251	69 166.6	$5p-18p-$
69 172.1 ($+J = 2$)	3	15.195	9.271	69 173.1	$5p-18p+$
69 222.4	~ 1	16.069	9.459	69 223.3	$5p-19p-$
69 227.0	~ 1	16.157	9.477	69 228.3	$5p-19p+$
69 270.5	~ 1.5	17.064	9.650	69 270.8	$5p-20p-$
69 274.2 ($+J = 2$)	1.6	17.148	9.665	69 275.3	$5p-20p+$
69 310.6	2	18.036	9.816	69 310.0	$5p-21p-$
69 313.7 ($+J = 2$)	2	18.135	9.832	69 314.7	$5p-21p+$
69 346.2	4	19.088	9.976	69 346.7	$5p-22p-$
		19.200	*9.992*	69 349.7	$5p-22p+$
69 364.8	8	19.706	10.061	69 367.6	$5p+13p+$
		20.136	*10.117*	69 376.7	$5p-23p-$
		20.202	*10.125*	69 378.5	$5p-23p+$
		20.806	*10.199*	69 393.8	$5p+13p-$
69 400.8	~ 1	21.113	10.235	69 401.2	$5p-24p-$

Table 3. *Continued.*

Experiment				Theory	
Energy (cm^{-1})	Width (cm^{-1})	$\nu_{1/2}$	$\nu_{3/2}$	Energy (cm^{-1})	Assignment
69 403.8 ($+J = 2$)	2	21.225	10.247	69 403.9	$5p - 24p+$
69 422.1	~ 1.5	22.071	10.338	69 422.6	$5p - 25p-$
(b $J = 2$)	2	22.179	10.349	69 424.5	$5p - 25p+$
69 441.3	~ 1	23.076	10.436	69 441.6	$5p - 26p-$
69 442.9 ($+J = 2$)	~ 1.5	23.166	10.445	69 443.2	$5p - 26p+$
69 458.0	~ 1	24.072	10.524	69 458.1	$5p - 27p-$
69 459.7 ($+J = 2$)	~ 1.4	24.181	10.533	69 459.7	$5p - 27p+$
69 472.7	~ 1	25.064	10.603	69 472.9	$5p - 28p-$
69 474.8 ($+J = 2$)	~ 1	25.151	10.609	69 474.3	$5p - 28p+$
69 485.3		26.020	10.672	69 485.9	$5p - 29p-$
69 486.8 ($+J = 2$)	2	26.141	10.680	69 487.2	$5p - 29p+$
nr		*27.060*	*10.740*	69 497.5	$5p - 30p-$
69 498.1 ($+J = 2$)	~ 1.5	27.113	10.743	69 498.7	$5p - 30p+$
nr		*28.044*	*10.799*	69 507.8	$5p - 31p-$
69 508.8 ($+J = 2$)	~ 1	28.140	10.804	69 509.0	$5p - 31p+$
nr		29.009	10.852	69 517.0	$5p - 32p-$
69 517.6 ($+J = 2$)	≤ 1	29.078	10.855	69 518.3	$5p - 32p+$
nr		29.885	10.896	69 524.5	$5p - 33p-$
69 526.3 ($+J = 2$)	≤ 1	30.105	10.906	69 526.6	$5p - 33p+$
nr		*31.123*	*10.953*	69 534.1	$5p - 34p-$
nr		*31.248*	*10.958*	69 535.0	$5p - 34p+$
nr		*32.095*	*10.993*	69 540.8	$5p - 35p-$
nr		*32.195*	*10.998*	69 541.5	$5p - 35p+$
nr		*33.060*	*11.030*	69 547.0	$5p - 36p-$
nr		*33.176*	*11.035*	69 547.7	$5p - 36p+$
(**) 69552	~ 15	33.919	11.062	(**) 69 555	$5p + 14p+$

[a]: Recorded only through the valence $4d5p\ ^1P_1$ intermediate state. **: Maximum of unresolved perturber envelope as observed through the $5s14p\ ^1P_1$ intermediate level with perpendicular laser polarizations. (b $J = 2$): blended by a $J = 2$ resonance. ($+J = 2$): superimposed with a $J = 2$ resonance. nr: not resolved. $: Strongly mixed levels. [c]: For experimentally unobserved energy levels the reported effective quantum numbers are calculated from the theoretical values and are given in italics.

the uncertainty is either the laser linewidth (~ 0.2 cm^{-1}) for narrow resonances, or the tenth of the level width for broad structures. Low lying levels, indicated with an [a] in Tables 2–4, were recorded exclusively through the $4d5p\ ^1P_1$ intermediate state. For the higher lying levels both valence and ICE techniques were used. However, the reported experimental data refer to measurements made using ICE. Theoretical energy level positions and their assignment were calculated from the $K_{\mathrm{eff},J}$ matrices restricted to closed channels (Eq. (5)).

4.3.1 The 5pnp J = 0 series

The $J = 0^e$ level structure below the $5p_{1/2}$ limit consists of two interacting Rydberg series, $5p_{1/2}np_{1/2}$ and $5p_{3/2}np_{3/2}$ (or $5p - np-$ and $5p + np+$ respectively in Table's 2 notation). Judged from their large widths these two series autoionize strongly into the three available continua, $5s\varepsilon s$, $4d_{3/2}\varepsilon d_{3/2}$ and $4d_{5/2}2\varepsilon d_{5/2}$. The theoretical Lu-Fano plot, $\nu_{1/2}$ (mod 1) *vs.* $\nu_{3/2}$, calculated from the $K_{\mathrm{eff},J=0}$ matrix restricted to closed channels, is shown in Figure 7a together with the experimental data (black dots). The agreement between experiment and calculation is quite satisfactory, as seen also from the differences between theoretical and experimental energies in Table 2 which are of the order of the level widths or smaller.

The presence of oblique branches in the Lu-Fano plot indicates that the two interacting closed channels are strongly mixed and that consequently their contributions to the wavefunctions have comparable weights. Similar

Table 4. $5pnp$ $J = 2$ series below the $5p_{1/2}$ Sr limit.

Experiment				Theory	
Energy (cm^{-1})	Width (cm^{-1})	$\nu_{1/2}$	$\nu_{3/2}$	Energy (cm^{-1})	Assignment
[a]63 171	87	4.116	3.883	63 138.7	$5p - 7p+$
[a]64 006	178	4.410	4.127	64 046.1	$5p + 7p-$
[a]64 280	193	4.522	4.218	64 311.0	$5p + 7p+$
[a]65 510	68	5.150	4.714	65 507.3	$5p - 8p+$
[a]66 264	90	5.695	5.121	66 284.5	$5p + 8p-$
[a]66 396	95	5.810	5.204	66 403.5	$5p + 8p+$
[a]66 777	57	6.183	5.467	66 779.0	$5p - 9p+$
		[c]*7.133*	[c]*6.090*	67 504.4	$5p - 10p + \$$
nr		*7.251*	*6.163*	67 548.3	$5p + 9p - \$$
[a]67 622	56	*7.361*	*6.231*	67 629.8	$5p + 9p + \$$
[a]67 999	18	8.159	6.693	67 999.0	$5p - 11p+$
[a]68 319	21	9.089	7.178	68 300.5	$5p + 10p-$
		9.120	*7.193*	68 324.2	$5p + 10p+$
[a]68 371 ($+J = 1$)	30	9.272	7.267	68 370.0	$5p - 12p+$
[a]68 585	13	10.163	7.673	68 585.1	$5p - 13p+$
68 765 ($+J = 1$)	22	11.152	8.073	68 768.2	$5p - 14p+$
		11.350	*8.147*	68 795.6	$5p + 11p-$
68 824	15	11.545	8.218	68 826.2	$5p + 11p+$
68 909	9	12.191	8.442	68 909.1	$5p - 15p+$
69 012.5	6	13.147	8.741	69 012.9	$5p - 16p+$
69 101 ($+J = 0, 1$)	~ 6	14.172	9.023	69 102.9	$5p - 17p+$
		14.645	*9.142*	69 135.7	$5p + 12p-$
69 150.6	~ 20	14.863	9.194	69 156.9	$5p + 12p+$
69 175 ($+J = 1$)	10	15.242	9.282	69 175.0	$5p - 18p+$
69 228.5 ($+J = 1$)	~ 1.8	16.186	9.483	69 228.5	$5p - 19p+$
69 275.2 ($+J = 1$)	~ 1.6	17.171	9.670	69 275.0	$5p - 20p+$
69 314.1 ($+J = 1$)	~ 1.2	18.146	9.834	69 312.5	$5p - 21p+$
69 347.0 ($+J = 0$)	2.2	19.114	9.980	69 350.3	$5p - 22p+$
69 376.6 ($+J = 0, 1$)	5	20.131	10.117	69 377.0	$5p - 23p+$
		20.379	*10.147*	69 383.1	$5p + 13p-$
69 394	11	20.811	10.200	69 395.2	$5p + 13p+$
69 405.6 ($+J = 1$)	4	21.304	10.256	69 405.1	$5p - 24p+$
69 424.0 ($+J = 1$)	~ 1.4	22.164	10.348	69 424.9	$5p - 25p+$
69 442.6 ($+J = 1$)	1	23.149	10.443	69 443.3	$5p - 26p+$
69 459.6 ($+J = 1$)	1	24.174	10.532	69 459.7	$5p - 27p+$
69 473.9 ($+J = 1$)	1	25.151	10.609	69 474.2	$5p - 28p+$
69 486.5 ($+J = 1$)	1	26.117	10.679	69 487.1	$5p - 29p+$
69 498.1 ($+J = 1$)	1	27.113	10.744	69 498.5	$5p - 30p+$
69 508.2 ($+J = 1$)	1	28.079	10.801	69 508.7	$5p - 31p+$
69 517.6 ($+J = 1$)		29.078	10.855	69 517.2	$5p - 32p+$
69 526.4 ($+J = 1$)		30.118	10.907	69 527.0	$5p - 33p+$
(b $J = 0$)		*31.297*	*10.960*	69 535.4	$5p - 34p+$
(b $J = 0$)		*32.214*	*10.998*	69 541.6	$5p - 35p+$
(b $J = 0$)		*33.192*	*11.035*	69 547.8	$5p - 36p+$
nr		*34.177*	*11.070*	69 553.4	$5p - 37p+$
nr		*35.161*	*11.102*	69 558.6	$5p - 38p+$
nr		*36.128*	*11.131*	69 563.3	$5p - 39p+$
nr		*37.179*	*11.162*	69 568.0	$5p - 40p+$
nr		*38.115*	*11.186*	69 571.8	$5p - 41p+$
nr		*39.005*	*11.208*	69 575.3	$5p - 42p+$
(**) 69 574	~ 43	38.671	11.200	(**) 69 577	$5p + 14p+$

[a]: Recorded only through the valence $4d5p\ ^1P_1$ intermediate state. **: Maximum of unresolved perturber envelope as observed through the $5s14p\ ^1P_1$ intermediate level with perpendicular laser polarizations. (b $J = x$): blended with a $J = x$ resonance. ($+J = x$): superimposed with a $J = x$ resonance. nr: not resolved. $: Strongly mixed levels. [c]: For experimentally unobserved energy levels the reported effective quantum numbers are calculated from the theoretical values and are given in italics.

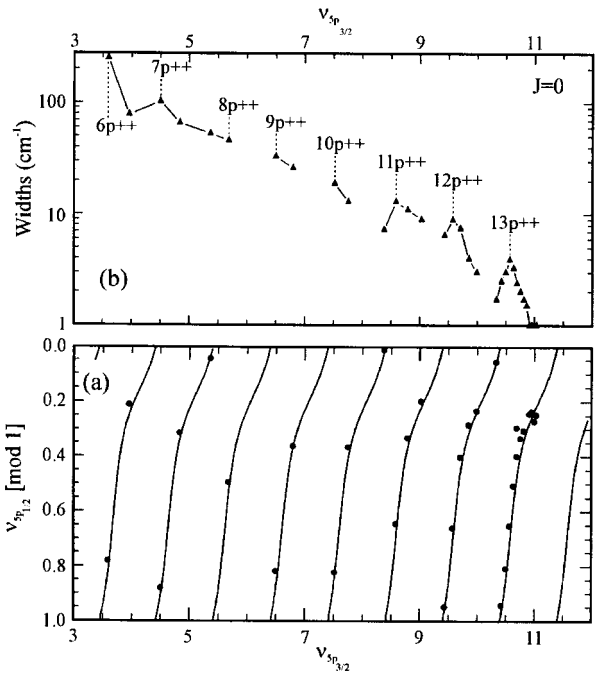

Fig. 7. (a) Lu-Fano plot of the $5pnp$ $J = 0$ levels of Sr. The curves are calculated with the help of the $K_{\mathrm{eff},J=0}$ matrix, while the experimentally observed energy levels are denoted by black dots (•). (b) Experimentally measured widths of the $5pnp$ $J = 0$ levels as a function of the effective quantum number $\nu_{3/2}$. The widths of the $[5p_{3/2}np_{3/2}]_{J=0}$ (np^{++}) perturbers are denoted with dashed lines.

strong mixing between two closed series was found for the $3dnd$ $J = 0$ series of Ca [25], for the $4fnf$ $J = 4$–6 spectra of Ba [26] and for the homologous $4pnp$ $J = 0$ series of Ca [13], while the mixing between the homologous $6p_{1/2}np_{1/2}$ and $6p_{3/2}np_{3/2}$ $J = 0$ series of Ba [11], although far from being negligible, is much weaker.

As one gets closer to the $5p_{1/2}$ limit, the Sr spectrum becomes dominated by $5p_{3/2}np_{3/2}$ perturbers, diluted in a number of $5p_{1/2}np_{1/2}$ members. In order to identify the $5p_{3/2}np_{3/2}$ levels one may observe the maxima of the ratio $R^{(n)} = [Z^{(n)}_{i+}/Z^{(n)}_{i-}]^2$, with $i+ \equiv 5p_{3/2}np_{3/2}$ and $i- \equiv 5p_{1/2}np_{1/2}$, for the channel admixture coefficients in the wavefunctions deduced from the $K_{\mathrm{eff},J=0}$ reaction matrix. The ratio $R^{(n)}$ oscillates between a maximum and a minimum value each one characterizing the dominance of the $5p_{3/2}np_{3/2}$ and the $5p_{1/2}np_{1/2}$ channel respectively. This criterion is very useful because it may characterize the $5p_{3/2}np_{3/2}$ perturber as being the most perturbed state even in the particular case where $R^{(n)}_{\max} < 1$. The maxima of $R^{(n)}$, occur near $\nu_{3/2}(\mathrm{mod}\ 1) \approx 0.55$. The strong mixing of the two closed channels is also reflected on the energy variation of the resonance widths, plotted in Figure 7b. Instead of constant scaled widths $\Gamma\nu_j^3$ for each channel, the data exhibit periodic (in the $\nu_{3/2}$ scale) oscillations, the maxima of which are located near the levels where $R^{(n)} = R^{(n)}_{\max}$.

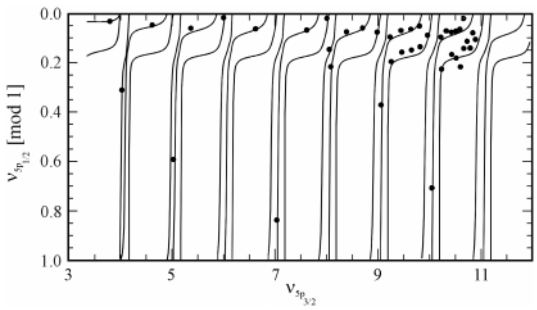

Fig. 8. Same as in Figure 7a for the Lu-Fano plot of the $5pnp$ $J = 1$ levels of Sr.

Apart from the six members with $n = 10$, 12, 14, 18, 23 and 24 which are either very weakly excited or blended with $J = 2$ resonances, the $5p_{1/2}np_{1/2}$ series was observed for $7 \leq n \leq 36$. Between the $4d_{5/2}$ and $5p_{1/2}$ limits the $5p_{3/2}np_{3/2}$ members have been recorded and identified for $6 \leq n \leq 13$. The $5p_{3/2}14p_{3/2}$ perturber is completely diluted into the highest members of the $5p_{1/2}np_{1/2}$ series, which are not resolved. It induces a broad resonance (~ 40 cm^{-1}) in the envelope of the unresolved $5p_{1/2}np_{1/2}$ resonances with a maximum near $n \sim 67$ (see $\sigma_{\|}$ in Fig. 5).

4.3.2 The 5pnp J=1 series

The $J = 1^e$ level structure consists of five closed channels, $5p_{1/2}np_{1/2}$, $5p_{1/2}np_{3/2}$, $5p_{3/2}np_{1/2}$, $5p_{3/2}np_{3/2}$ and $5p_{3/2}nf_{7/2}$ autoionizing into eight available continua. The Lu-Fano plot calculated from the $K_{\mathrm{eff},J=1}$ matrix, together with the experimental data (black dots) are shown in Figure 8. This Lu-Fano plot as well as the one for $J = 2$ includes the theoretical branches associated with the $5pnf$ series, which interact slightly with the $5pnp$ ones, although no quantitative information can obtained for the broad $5pnf$ resonances from the $K_{J,\mathrm{eff}}$ matrices built for a reaction volume with $r_0 = 20$ a.u. (see Sect. 3).

The observed levels are attributed to the three series $5p_{1/2}np_{1/2}$, $5p_{1/2}np_{3/2}$ and $5p_{3/2}np_{3/2}$ (see Tab. 3). The $5p_{3/2}np_{1/2}$ series are absent from the ICE spectra due to cancellation effects in the transition matrix element. In the valence spectra this series is not observed because it is blended with the $J = 2$ lines. The $5p_{1/2}14p_j$ and $5p_{3/2}11p_j$ resonances are strongly mixed making meaningless their identifications.

The $J = 1$ series are weakly coupled resulting in nearly constant quantum defects $\mu = 2.93$ and 2.85 and $\mu = 2.94$ for the $5p_{1/2}np_{1/2}$, $5p_{1/2}np_{3/2}$ and $5p_{3/2}np_{3/2}$ series respectively. The last resonance $5p_{3/2}14p_{3/2}$ below the $5p_{1/2}$ threshold is strongly coupled to the members of the $[5p_{1/2}np]_J$ series for $n \sim 34$ giving rise to an unresolved structure with a width of ~ 15 cm^{-1}. Similar weak mixing between $J = 1$ series was found for the $6pnp$ $J = 1$ series of Ba [11,12].

Due to the extensive superposition of the $J = 1$ lines with the $J = 2$ ones a detailed study of the $J = 1$ resonant widths can not be given. As a general remark the $J = 1$ states are fairly sharp. Especially the $5p_{1/2}np_j$ resonances

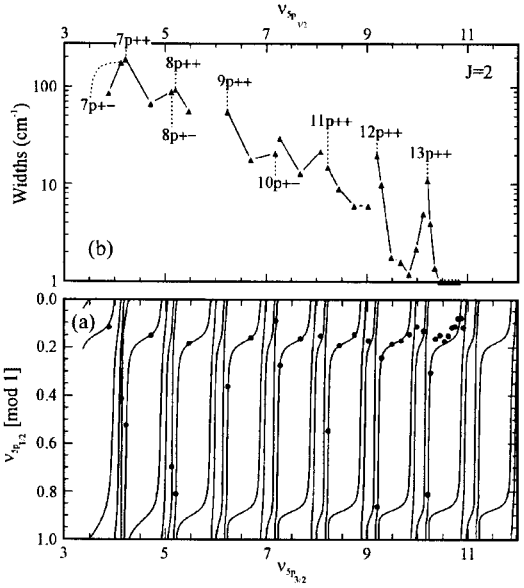

Fig. 9. (a) Same as in Figure 7a for the Lu-Fano plot of the $5pnp$ $J = 2$ levels of Sr. (b) Experimentally measured widths of the $5pnp$ $J = 2$ levels as a function of the effective quantum number $\nu_{3/2}$. The widths of the $[5p_{3/2}np_{3/2}]_{J=2}$ (np^{++}) and the observed $[5p_{3/2}np_{1/2}]_{J=2}$ (np^{+-}) perturbers are denoted with dashed lines.

near the $5p_{1/2}$ limit have widths of the order of 1 cm^{-1} or less. Such small widths have been observed also in the homologous series of Ba [11,12] and Ca [13].

4.3.3 The 5pnp J=2 series

The $J = 2^e$ level structure consists of six closed channels, $5p_{1/2}np_{3/2}$, $5p_{3/2}np_{1/2}$, $5p_{3/2}np_{3/2}$, $5p_{1/2}nf_{5/2}$, $5p_{3/2}nf_{5/2}$ and $5p_{3/2}nf_{7/2}$ autoionizing into eleven available continua.

The Lu-Fano plot calculated from the $K_{\mathrm{eff},J=2}$ matrix, together with the experimental data are shown in Figure 9a. The observed levels are classified into two series identified as $5p_{1/2}np_{3/2}$ and $5p_{3/2}np_{3/2}$. As can be noted in Table 4 the third $5pnp$ channel, $5p_{3/2}np_{1/2}$, was not observed apart from the two levels at 64 006 cm^{-1} $(5p_{3/2}7p_{1/2})$ and 66 264 cm^{-1} $(5p_{3/2}8p_{1/2})$ appearing in the valence spectra as shoulders of the much stronger lines corresponding to the $5p_{3/2}7p_{3/2}$ (see Fig. 2) and $5p_{3/2}8p_{3/2}$ levels. The absence of the $5p_{3/2}np_{1/2}$ members from the excitation cross-section (valence as well as ICE) is in agreement with the calculations, which give strongly destructive interference effects in the excitation of the $5p_{3/2}np_{1/2}$ resonances. For example for the $6s13p \rightarrow 5p_{3/2}np_{1/2}$ transition, the intensities calculated by disregarding the interference effects, *i.e.* by calculating the quantity $\Sigma_\rho \square \Sigma_i |Z_{i\rho} D_i|^2$, are about 4.5 times larger than the values obtained from the exact formula (Eq. (3)) $\Sigma_\rho |\Sigma_i Z_{i\rho} D_i|^2$. The latter formula accounts, for each physical wavefunction ρ, for the interference effects between the contributions due to the different ionization channels i. On the opposite, interference effects are almost negligible in the excitation of the $5p_{3/2}np_{3/2}$ resonances, the corresponding ratio being ~ 1.

The Lu-Fano plot of Figure 9a reveals small discrepancies between theory and experiment; nevertheless the agreement is quite satisfactory, with most of the differences remaining smaller than the experimental widths. However, level positions computed using the $K_{\mathrm{eff},J=2}$ matrix do not always coincide with the corresponding level maxima obtained from the theoretical cross-sections. The latter are closer to the experimental values reported in Table 4. The Lu-Fano plot shows that the various $J = 2$ channels are weakly coupled to each other. Similar weak channel mixing was observed for the homologous $6pnp$ series of Ba [11,12]. The $5p_{3/2}nl$ channels cause relatively weak perturbations of the $5p_{1/2}np_{3/2}$ series, whose quantum defect varies around the value $\mu \approx 2.84$. A significant number of $5p_{1/2}np_{3/2}$ members ($n \sim 14$–15, $n \sim 17$–18, $n \sim 23$–24) interacts with the $5p_{3/2}n'p_{3/2}$ perturbers with $n' = 11$–13, making this quantum defect variation more noticeable there. The $5p_{3/2}14p_{3/2}$ perturber is diluted among the high members of the $[5p_{1/2}np]_J$ series around $n \sim 34$ giving rise to an unresolved structure with a width of ~ 43 cm^{-1}. The identification of the $5p_{3/2}np_{3/2}$ members, with $n = 11$, 12 and 13 is quite straightforward, their quantum defect being nearly constant $\mu \approx 2.8$. The above quantum defect-based analysis is supported by the behavior of the observed linewidths shown in Figure 9b which appear to be even more sensitive than the quantum defects. The two observed $5p_{3/2}7p_{1/2}$ and $5p_{3/2}8p_{1/2}$ levels have almost identical $\Gamma\nu_{3/2}^3 \approx 12\,300$ cm^{-1} values comparable in magnitude to those of the $5p_{3/2}np_{3/2}$ channel. Most of the $5p_{1/2}np_{3/2}$ members in the range $0.5 \leq \nu_{3/2}(\mathrm{mod}\ 1) \leq 1$ exhibit a nearly unperturbed scaled width $\Gamma\nu_{1/2}^3 \approx 8\,100$ cm^{-1}. For $0.0 \leq \nu_{3/2}(\mathrm{mod}\ 1) \leq 0.15$ the rather sudden increase of the widths of the $5p_{1/2}np_{3/2}$ members reflects the mixing with $5p_{3/2}np_{3/2}$ levels having scaled widths which are approximately 60% larger.

The $5pnf$ channels cannot be excited directly under the employed ICE scheme while this is possible when excitation takes place through the $4d5p$ $^1\mathrm{P}_1$ intermediate state. In the latter case only a few very broad and weak $5p_{3/2}nf_j$ resonances appear. Although these experimentally observed resonances are not included in the Lu-Fano plot of Figure 9a, their quantum defect $\mu \sim 0.05$ suggests that they mostly perturb the $5p_{1/2}np_{3/2}$ levels with $n = 14$ and 17.

5 Conclusions

The experimental and theoretical study of the even-parity $5p_{1/2,3/2}np$ $J = 0$–2 autoionizing states of strontium has been presented. The major part of the recordings and the theoretical analysis have been focused on the two-step $5s^2\ ^1\mathrm{S}_0 - \lambda_1 \rightarrow 5sn'p\ ^1\mathrm{P}_1$ $(n' = 12$–$16) - \lambda_2 \rightarrow [5p_{3/2}np]_J$ Isolated Core Excitation scheme. The use of such a limited number of intermediate $5sn'p\ ^1\mathrm{P}_1$ bound Rydberg states has been dictated by the strong mixing of this series with

the $4d5p\ ^1P_1$ level for $n < 12$ and by the non-availability of the necessary excitation wavelengths for $n > 16$. Despite that, it was made possible to cover an extended energy-range below as well as above the $5p_{1/2}$ threshold by using the $5s \rightarrow 5p_{3/2}$ ionic transition and by applying the "Power-spectrum" technique. The resonances corresponding to the $5p_{1/2}np$ states showed up in the spectra through their mixing with the $5p_{3/2}np$ ones. The inconvenience of the "Power-spectrum" technique, namely the deformation of the spectral features near the ICE overlap integral zeros (especially above the $5p_{1/2}$ threshold) has been eased by the comparison of the ICE spectra with those obtained from the application of a different two-step excitation scheme *via* the bound $4d5p\ ^1P_1$ level. The latter scheme has also been used to populate the low-lying $5pnp$ levels, for the excitation of which ICE is not well suited, as well as some $5pnf$ levels.

J-identification of the observed structures has been achieved using two different combinations of the linear polarizations (mutually parallel and perpendicular) of the exciting laser beams and analyzing the theoretical excitation profiles calculated by the eigenchannel R-matrix method coupled to the MQDT formalism. The detailed comparison between experimental and theoretical spectra has been quite decisive for the analysis, due to the extensive superposition of resonances with different J values. Recorded and calculated ICE profiles are in very good agreement in the whole energy-range covered. Moreover, theory predicted the inefficient excitation of the two experimentally unobserved $5p_{3/2}np_{1/2}$ $J = 1$ and $J = 2$ series, attributing it to cancellation effects in the transition matrix element. Thus, only seven out of the nine existing $5pnp$ $J = 0$, 1, 2 series have been observed and identified for $6 \leq n \sim 35$, completing the previous work in Sr which concerned the $5p6p$ levels below the $4d_{3/2}$ threshold. The perturbation of the $5p_{1/2}np$ series by the $5p_{3/2}np$, $n = 6{-}14$, states of the same J value has been followed by observing the variation of quantum defects (Lu-Fano plots) and level widths (for $J = 0$ and 2) as a function of energy. The agreement between observed and calculated (from the $K_{\mathrm{eff},J}$ matrix) energy level positions has been found quite satisfactory since, in all cases, the differences were of the order of the level widths or less. The level widths have been found to exhibit drastic variations in the neighborhood of the perturbers.

The present study has completed the spectroscopy of the lowest $mpnp$ autoionizing series of alkaline-earth atoms. Electron correlations in the $5pnp$ series have been compared and found to exhibit, for a given J value, a similar behavior with those analyzed in the homologous $4pnp$ series of calcium and $6pnp$ series of barium. The $J = 0$ closed channels are strongly coupled to each other as well as with the available continua. The interaction is much weaker in the $J = 1$ and $J = 2$ closed channels. The $J = 1$ series additionally exhibit fairly narrow widths.

An open question that has not been addressed here concerns the deeper understanding of the autoionization mechanisms and the knowledge of the final states of the ion core and the ejected electron. This information may be obtained from energy and angular distribution measurements of the produced photoelectrons. Such measurements for the $mpnp$ series would be worthwile to undertake not only in strontium but also in barium and calcium, where, to our knowledge, there are no data available. Towards such an experimental project we are currently working.

Numerical calculations were carried out on the Cray 98 belonging to the "Institut de Développement des Ressources en Informatique Scientifique" of the French "Centre National de la Recherche Scientifique". The "Laboratoire Aimé Cotton" is associated with the Université Paris-Sud.

References

1. M. Aymar, C.H. Greene, E. Luc-Koenig, Rev. Mod. Phys. **68**, 1015 (1996).
2. A. Bolovinos, A. Jimoyiannis, S. Assimopoulos, P. Tsekeris, J. Phys. B: At. Mol. Opt. Phys. **25**, L533 (1992); S. Assimopoulos, A. Bolovinos, A. Jimoyiannis, P. Tsekeris, E. Luc-Koenig, M. Aymar, J. Phys. B: At. Mol. Opt. Phys. **27**, 2471 (1994); E. Luc-Koenig, A. Bolovinos, M. Aymar, S. Assimopoulos, A. Jimoyannis, P. Tsekeris, Z. Phys. D **32**, 49 (1994).
3. M. Kompitsas, S. Cohen, C.A. Nikolaides, C.A. Robaux, M. Aymar, P. Camus, J. Phys. B: At. Mol. Opt. Phys. **23**, 2247 (1990); A. Jimoyannis, A. Bolovinos, P. Tsekeris, Z. Phys. D **22**, 557 (1992); A. Jimoyannis, A. Bolovinos, P. Tsekeris, P. Camus, Z. Phys. D **25**, 135 (1993).
4. M. Kompitsas, S. Goutis, M. Aymar, P. Camus, J. Phys. B: At. Mol. Opt. Phys. **24**, 1557 (1991).
5. S. Goutis, M. Aymar, M. Kompitsas, P. Camus, J. Phys. B: At. Mol. Opt. Phys. **25**, 3433 (1992).
6. P. Camus, M. Dieulin, A.E. Himdy, M. Aymar, Phys. Scripta **27**, 125 (1983); C.J. Dai, S.M. Jaffe, T.F. Gallagher, J. Opt. Soc. Am. B **6**, 1486 (1989); R. van Leeuwen, W. Ubachs, W. Hogervost, J. Phys. B: At. Mol. Opt. Phys. **27**, 3891 (1994) and references therein.
7. J. Bokor, R.R. Freeman, W.E. Cooke, Phys. Rev. Lett. **48**, 1242 (1982); S.E. Harris, Phys. Rev. Lett. **62**, 1033 (1989); A. Lyras, X. Tang, P. Lambropoulos, J. Zhang, Phys. Rev. A **40**, 4131 (1989).
8. C.C. Chu, H.S. Fung, H.H. Wu, T.S. Yih, J. Phys. B: At. Mol. Opt. Phys. **31**, 3843 (1998).
9. R. Kachru, H.B. van Linden van den Heuvel, T.F. Gallagher, Phys. Rev. A **31**, 700 (1985).
10. T.F. Gallagher, *Rydberg Atoms* (Cambridge University Press, 1994).
11. B. Carré, P. d'Oliveira, P.R. Fournier, F. Gounand, M. Aymar, Phys. Rev. A **42**, 6545 (1990); J.G. Story, E.G. Yap, W.E. Cooke, Phys. Rev. A **39**, 5127 (1989).
12. E. Luc-Koenig, M. Aymar, J. Phys. B: At. Mol. Opt. Phys. **24**, 4323 (1991).
13. A. Bolovinos, E. Luc-Koenig, S. Assimopoulos, A. Lyras, N.E. Karapanagioti, D. Charalambidis, M. Aymar, Z. Phys. D **38**, 265 (1996).
14. K.T. Lu, Proc. Roy. Soc. **353**, 431 (1977); N. Vaeck, M. Godefroid, J.E. Hansen, Phys. Rev. A **38**, 2830 (1988) and references quoted in [1].
15. H.G. Werij, C.H. Greene, C.E. Theodosiou, A. Gallagher, Phys. Rev. A **46**, 1248 (1992).

16. U. Fano, A.R.P. Rau, *Atomic Collisions and Spectra* (Academic, Orlando, 1986).
17. A. Giusti-Suzor, U. Fano, J. Phys. B: At. Mol. Opt. Phys. **17**, 215 (1984); W.E. Cooke, C.L. Cromer, Phys. Rev. A **32**, 2725 (1985).
18. J.M. Lecomte, J. Phys. B: At. Mol. Opt. Phys. **20**, 3645 (1987).
19. M. Aymar, J.M. Lecomte, J. Phys. B: At. Mol. Opt. Phys. **22**, 223 (1988).
20. S.A. Bhatti, C.L. Cromer, W.E. Cooke, Phys. Rev. A **24**, 161 (1981).
21. E. Luc-Koenig, M. Aymar, J.M. Lecomte, A. Lyras, J. Phys. B: At. Mol. Opt. Phys. **31**, 727 (1998).
22. S. Cohen, Eur. Phys. J. D **4**, 31 (1998).
23. R.J. de Graaff, W. Ubachs, W. Hogervost, M. Abutaleb, Phys. Rev. A **42**, 5473 (1990).
24. E.A.J.M. Bente, W. Hogervost, J. Phys. B: At. Mol. Opt. Phys. **23**, 1403 (1990); M. Abutaleb, R.J. de Graaff, W. Ubachs, W. Hogervorst, Phys. Rev. A **44**, 4187 (1991).
25. M. Aymar, M. Telmini, J. Phys. B: At. Mol. Opt. Phys. **24**, 4935 (1991).
26. E. Luc-Koenig, M. Aymar, J.M. Lecomte, J. Phys. B: At. Mol. Opt. Phys. **27**, 2447 (1994).